

M. PITTMAN[✉]
S. FERRÉ
J.P. ROUSSEAU
L. NOTEBAERT
J.P. CHAMBARET
G. CHÉRIAUX

Design and characterization of a near-diffraction-limited femtosecond 100-TW 10-Hz high-intensity laser system

Laboratoire d'Optique Appliquée, ENSTA, Ecole Polytechnique, CNRS UMR 7639, Chemin de la Hunière, 91 761 Palaiseau Cedex, France

Received: 4 January 2002

Published online: 14 May 2002 • © Springer-Verlag 2002

ABSTRACT We present the design and characterization of a femtosecond high-intensity laser system emitting a near-diffraction-limited beam. This system was dimensioned in order to reach intensities in excess of 10^{20} W/cm² at a high repetition rate for ultrahigh-field physics experiments. We describe the improvements that were added to a conventional chirp pulse amplification configuration in order to decrease the deleterious effects of gain narrowing, gain shifting, thermal focusing in the amplifier stages, and spatial degradation due to multipass amplification processes.

PACS 42.60.By; 42.65.Re; 42.60.Jf; 42.60.Da; 01.52.tr

1 Introduction

Currently, high peak power laser systems can produce the high intensities required for many high-field applications such as plasma physics, coherent X-ray generation, or high-harmonic generation [1]. Owing to the combination of efficient broadband laser materials such as titanium-doped sapphire (Ti:Sa) with the associated techniques of Kerr-lens mode locking and the chirp pulse amplification (CPA) method [2], femtosecond laser systems have become the primary method to reach very high intensities. The ability to stretch ultrashort pulses with no optical aberration [3], to amplify pulses over more than nine orders of magnitude, and to compress amplified chirped pulses by re-compensating the spectral phase of the induced chirp up to the third order result in energies at the joule scale in tens of femtoseconds with corresponding peak powers as high as 100 TW [4]. The only alternative method for producing such high peak powers, namely amplification of longer subpicosecond pulses to energies ranging from hundreds of joules up to kilojoules [5, 6], leads to giant and expensive installations well beyond the abilities of most laboratories. Such systems are still based on CPA, but the output spectra are limited to about 5 nm by the bandwidth of the high energy amplifying materials used to reach kilojoule levels, namely Nd:phosphate glass. Moreover, the repetition rates of such systems are limited to a few shots

per hour due to the poor thermal conductivity of Nd:glass materials.

However, in order to produce high-energy femtosecond pulses (i.e. at the joule scale), it is necessary to overcome the following two parasitic phenomena, which are due to the high amplification level. First, pre-amplification in either regenerative or multipass configuration, which allows a high energy gain of more than 10^6 , induces a narrowing of the initial laser spectrum with respect to the stimulated emission cross section of the amplifying medium (centred around 780 nm for Ti:sapphire). Moreover, the successive power amplifier stages shift the spectrum to the red because of the gain saturation: the red component of the chirped pulses traveling in the leading position benefits from a larger population inversion than the following ones, leading thereby to a stronger amplification. An interesting approach in order to counteract these spectral distortions consists in choosing the input laser spectrum so as to make spectral narrowing and gain saturation compensate for each other during the amplification process [7].

The second major problem due to amplification in high-peak-power laser systems deals with the thermal effects induced by the strong average pump power in the last amplifier crystal. The heating of the laser medium produces a spatially dependent increase of its refractive index, determined by the transverse energy distribution of the pump beam and the intrinsic thermo-mechanical properties of the medium, thereby leading to unwanted thermal lensing of the amplified beam. This effect can be more or less compensated for by the use of a negative lens, but this is essentially a 'point design' where a particular focal length is chosen in order to compensate for a given temperature, and leads to a strong thermal dependence of the amplifier that prevents pumping modifications. Moreover, transverse inhomogeneities of the pumping energy induce local heating of the crystal and distort the wavefront of the amplified pulse.

In this paper, we present an ultrahigh-intensity CPA system based on our previously reported high-peak-power laser [8, 9] with substantially increased performance, allowing us to move from the 30-TW to the 100-TW scale while keeping the same repetition rate. In addition, with the design of a new multipass high-power amplifier, allowing stronger amplification, we implemented two major changes in order to counteract the previously described drawbacks. The spectral narrowing and distortions due to amplification were balanced

✉ Fax: +33-169/3199-96, E-mail: pittman@ensta.ensta.fr

by using an actively controlled acousto-optic programmable dispersive filter (AOPDF) in order to obtain output pulses shorter than 25 fs. The thermally induced spatial distortions were efficiently suppressed by housing the final power amplifier crystal in a cryogenic chamber. An almost complete characterization of the system is presented, evidencing the effects of the improvements on the temporal, the spatial, and the wavefront profiles of the amplified beam. Thanks to these implementations, the system delivers a near-diffraction-limited beam, which allows us to reach intensities greater than 10^{20} W/cm² when focused with a 300-mm off-axis parabola.

2 Laser setup

The laser system is based on a classical CPA configuration (see Fig. 1). From the front end up to the output of the second amplifier stage, it is similar to our previously presented system [8, 9].

2.1 Overall CPA layout

The laser chain starts from a Ti:sapphire self-mode-locked oscillator pumped with 6 W CW delivered by an argon-ion laser. The oscillator produces an 88-MHz 300-mW train of pulses of 15-fs duration. Each pulse is first stretched up to 400 ps in an aberration-free stretcher based on an Öffner-triplet design [3]. Pulses then pass through the AOPDF, which allows us to actively control the spectral shape and to adjust the spectral phase (see Sect. 2.2 below), and through a pulse picker which selects pulses at a repetition rate of 10 Hz. The 1-nJ pulses are sent into a 8-pass pre-amplifier in order to reach 2 mJ and then pass through a second Pockels cell, which acts both as a back-reflection isolator and a temporal gate which limit the amplified spontaneous emission (ASE) energy. After that, the pulses are amplified through the 5-pass

power amplifier in order to reach an energy of 200 mJ. After each of these two amplification steps the beam is spatially filtered and up-collimated through a 4× magnification beam expander in order both to increase the spatial quality of the IR beam [10] and to limit its fluence (i.e. carried energy relative to the section of the beam) below the damage threshold of the following optics, especially the crystal of the next amplifier.

Pulses are then amplified through the third amplifier up to an energy of 3.5 J after four passes. This high-power amplification stage has been upgraded by the addition of a cryogenic cooling chamber (detailed in Sect. 2.3 below) canceling the thermal dependence of the wavefront of the amplified beam. After this last amplifier stage, the beam is sent into a 2-m-diameter vacuum chamber where it is collimated up to 60-mm diameter (top-hat transverse profile) using a 3× aberration-free off-axis parabolic mirror beam expander. Finally, the pulses are re-compressed to 25 fs after four passes on two parallel gratings. The output energy is 2.5 J, which leads to 100-TW peak power.

2.2 Active spectral optimization

In order to pre-compensate for the spectral modifications, which are gain narrowing and gain shifting induced by the amplification processes in addition to the spectral phase changes due to the propagation, we chose to introduce a programmable acousto-optic dispersive filter ('DAZZLER', Fastlite, France) after the stretcher (see Fig. 1). This device allows us to control the spectral amplitude and phase of the pulse by interacting the laser light with a longitudinally traveling acoustic wave [11, 12]. The polarization of the diffracted beam is rotated by 90° along the extraordinary index of the acousto-optic crystal. The operating principle is illustrated in Fig. 2.

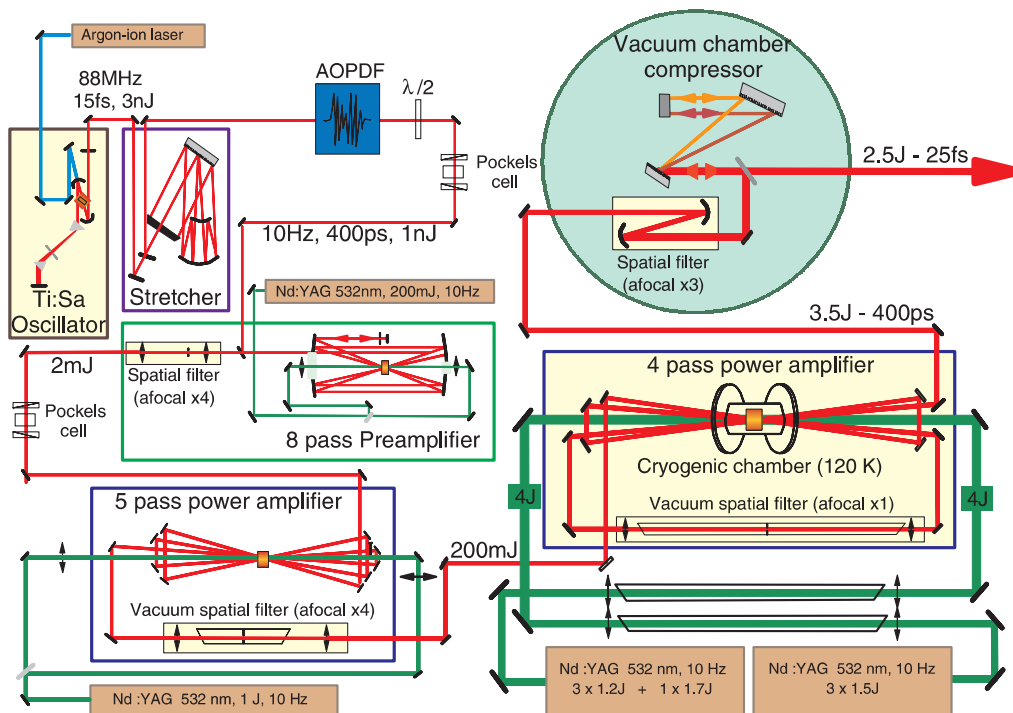


FIGURE 1 The 100-TW laser setup

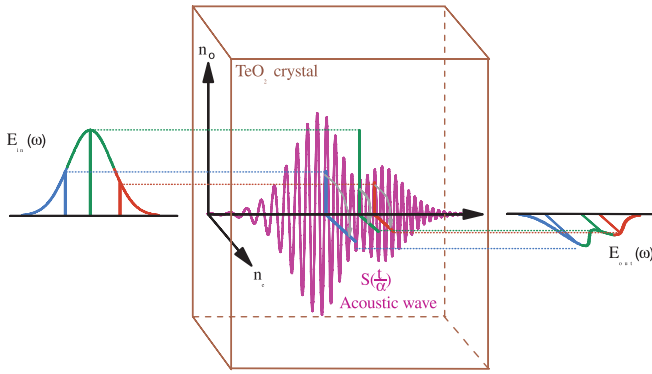


FIGURE 2 Principle of the acousto-optic programmable dispersive filter. The longitudinally propagating acoustic wave can be modulated both in time – or frequency domain – and amplitude. It diffracts the in-phase optical spectral components traveling through the crystal at different propagation distances inside the crystal. The interacting depth is shifted with the frequency modulation in order to adjust the output optical spectral phase. The diffraction efficiency of each optical spectral component depends on the amplitude of the interacting acoustic wave. In this example, the central component is diffracted with a lower efficiency than the left and the right ones, thus leading to a dip at the center of the output spectral profile. In addition, each component is diffracted in the crystal at a given location determined to provide the useful phase shift

By modulating the amplitude of the traveling acoustic wave (which is essentially stationary by comparison with the traveling optical wave), one can adjust the diffraction efficiency for each phase-matched optical spectral component in accordance with the following relation:

$$E_{\text{out}}(t) = E_{\text{in}}(t) \otimes S\left(\frac{t}{\alpha}\right) \quad \text{in the time domain,} \quad (1)$$

which can be written

$$E_{\text{out}}(\omega) = E_{\text{in}}(\omega) \times S(\alpha\omega) \quad \text{in the frequency domain,} \quad (2)$$

where $\alpha = \Delta n(V/c)$ is the ratio of sound to light velocities times the index mismatch between ordinary and extraordinary waves, $S(t)$ ($S(\omega)$) is the temporal (frequency-domain) acoustic wave, and $f \otimes g$ is the convolution of the functions f and g . In the same way, by modulating the frequency of the acoustic wave, one can adjust the longitudinal position in the crystal where the diffraction occurs for each spectral component in order to tune the phase dispersion. This can be achieved independently for each dispersion term up to the fourth order.

The AOPDF is externally triggered at a frequency of 10 Hz in order to reduce the average power of the acoustic signal sent into the crystal. In this configuration, we measured a transmission efficiency of the AOPDF greater than 90% when no amplitude modulation of the acoustic wave is applied. A typical modulation applied to the laser spectrum for gain-narrowing pre-compensation is shown in Fig. 3.

Moreover, beyond the possibility to control and minimize the output pulse duration, another advantage of the AOPDF consists in achieving an active control of the laser–target interaction by modifying the input spectro-temporal characteristics so as to reshape the pulse profile, optimize the pulse duration, or create a pre-pulse within a limited time window of 3 ps.

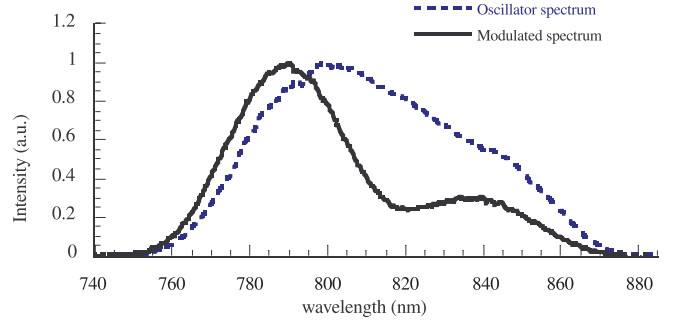


FIGURE 3 Typical oscillator spectrum and AOPDF output modulated spectral shape injected in the amplifier chain

2.3 Cryogenic-cooling amplification system

In order to reach the energy level required to obtain the output power of 100 TW, the pumping power of the third power amplifier stage has been increased up to 80 W at 10 Hz. In the previous configuration, this amplification stage was pumped at 10 Hz by 4 J of the second harmonic delivered by three commercial flash-pumped Nd:YAG lasers (GCR-350 from Spectra-Physics, max. 1.5 J). We chose to keep the same strategy by adding four commercial Nd:YAG lasers (1 GCR-350 PRO, max. 1.7 J, and three SAGA from Thales Laser, max. 1.2 J). The available pump power was increased to almost 100 W, thus leading to a maximum amplified pulse energy of 3.5 J before compression. However, such a high average power induces a strong heating of the crystal. This produces a spatially dependent gradient of the refractive index of the crystal in the pumping zone and leads to an unwanted focusing of the amplified beam. Moreover, inhomogeneities in the transverse intensity profile and mechanical deformations due to thermo-mechanical stress of the crystal lead to local index variations, which degrade the amplified pulse wavefront. These effects were measured using the Shack–Hartmann (SH) wavefront technique when using standard water cooling for two pumping powers of 40 W and 80 W; the corresponding focal spot transverse profiles (point spread functions ‘PSF’) calculated for a focal length of 300 mm are presented in Fig. 4.

These absolute SH measurements evidence that the increasing pump power into the crystal strongly deteriorates the wavefront of the amplified pulse, leading thereby to a poor beam quality and subsequent focusing. We have investigated the solution consisting in cooling the crystal down to cryogenic temperature (120 K), in order to increase its thermal conductivity while reducing both the refractive-index gradient and the thermo-mechanical stress.

The crystal is housed in a vacuum chamber which is closed on both sides by two 100-mm – diameter glass windows oriented at the Brewster angle (see Fig. 5). The cooling is achieved by using a closed-loop circulation of a special cryogenic gas mixture through the three drilled copper holders of the 30-mm diameter \times 20 mm Ti:sapphire crystal. This PT-16 gas (Praxair Technology, Inc.) was chosen for its ability to cool down to 120 K with a capacity of about 20 W per cold end.

In order to quantify the effects of cryogenic cooling, we compared the wavefront of the amplified beam we meas-

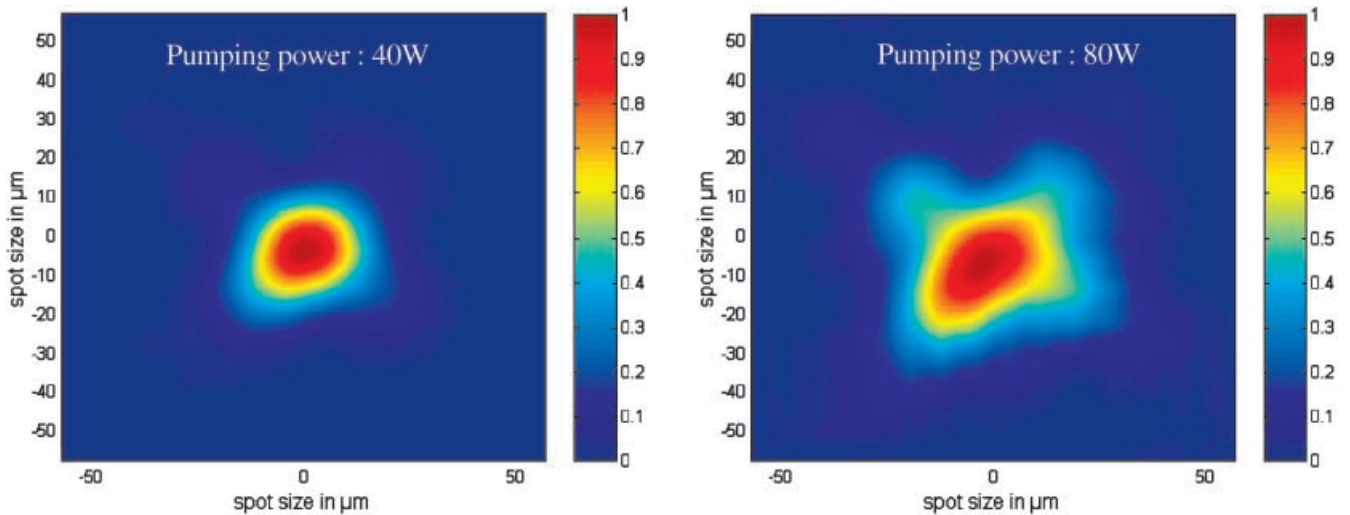


FIGURE 4 Focal spots of the amplified beam calculated from absolute Shack–Hartmann wavefront measurements for two average pumping powers of the Ti:sapphire crystal of 40 W (*left*) and 80 W (*right*). The increasing pumping power leads to a severe spatial distortion of the amplified beam

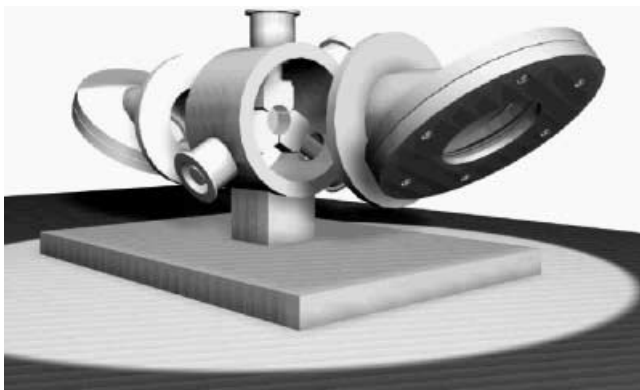


FIGURE 5 3D representation of the vacuum cryogenic chamber. The cylindrical crystal amplifier is maintained by three drilled copper holders through which the cryogenic gas circulates. The chamber is closed on both sides by Brewster windows

ured in the case of water cooling (300 K) and of cryogenic cooling (120 K) with the 80-W pumping power. To consider only the thermally induced pumping effects, these measurements were made relatively to the incident unamplified beam under two amplifying conditions for each cooling configuration. In the first condition we delayed the IR pulse 10 μs after the pump, in order to reduce the extracted energy and so maximize the heat emission (the excited-state lifetime of the Ti:sapphire crystal being of the order of 3 μs at room temperature and up to 3.8 μs at 120 K [13, 14]), leading thereby to the worst conditions with expected strong wavefront distortions. In the second condition, we tuned the delay between IR and pump pulses in order to optimize amplification, thus leading to a decrease of temperature due to the strong excited-state depletion. The corresponding ‘thermally dependent’ calculated PSFs are presented in Fig. 6.

These measurements confirm the strong wavefront distortion due to the heating of the crystal, the degradation of the calculated focal spot being of greater importance in the case of the low amplification for each cooling configuration. Moreover, it evidences the efficiency of cryogenic cooling in order to keep good spatial characteristics. The calculated equiva-

lent wavefront distortions in terms of thermal lens effects and thermally induced optical aberrations are presented in Table 1.

These calculations underline that cryogenic cooling leads to negligible thermal focusing and low aberrations up to the seventh order. The Strehl ratio (SR) (i.e. intensity ratio between the real peak intensity and the peak intensity calculated for the same transverse intensity distribution with a flat wavefront) shows that cryogenic cooling allows us to maintain the maximum peak intensity to more than 90% after the third amplification stage (assuming an incident beam with $\text{SR} = 1$). By contrast, when using classical water cooling, more than 85% of the intensity ($\text{SR} = 13\%$) is spread out of the peak because of the thermally induced wavefront distortion.

3 Output-pulse characterization

3.1 Temporal considerations

Temporal measurements were made after compression and for maximum amplification by using the SPIDER technique [15, 16], in order to optimize AOPDF spectral and phase pre-compensation. Figure 7 shows spectral intensities and phases we measured in the cases when we applied AOPDF pre-correction only for the output phase and for both amplitude and phase output optimizations by comparison with a non-pre-compensated output pulse. The input spectra, for both cases (with and without spectral shaping), are the ones presented in Fig. 3.

By calculating the inverse complex Fourier transform, the SPIDER method gives the pulse-intensity profiles represented in Fig. 8. By applying only phase pre-correction, we are able to flatten the output spectral phase better than 0.5 rad peak-to-valley all over the spectrum, especially in the wings where the uncorrected phase exhibits strong modulations (larger than 4 rad peak-to-valley). This leads to a decrease of the output-pulse duration of more than 20%, from 34 fs FWHM down to 27 fs as well as an increase of the intensity of about 10%.

When the input spectral intensity is modulated, the output spectrum is broadened over more than 45%, from 35 nm FWHM up to 54 nm with a quasi-fourth-order super-Gaussian

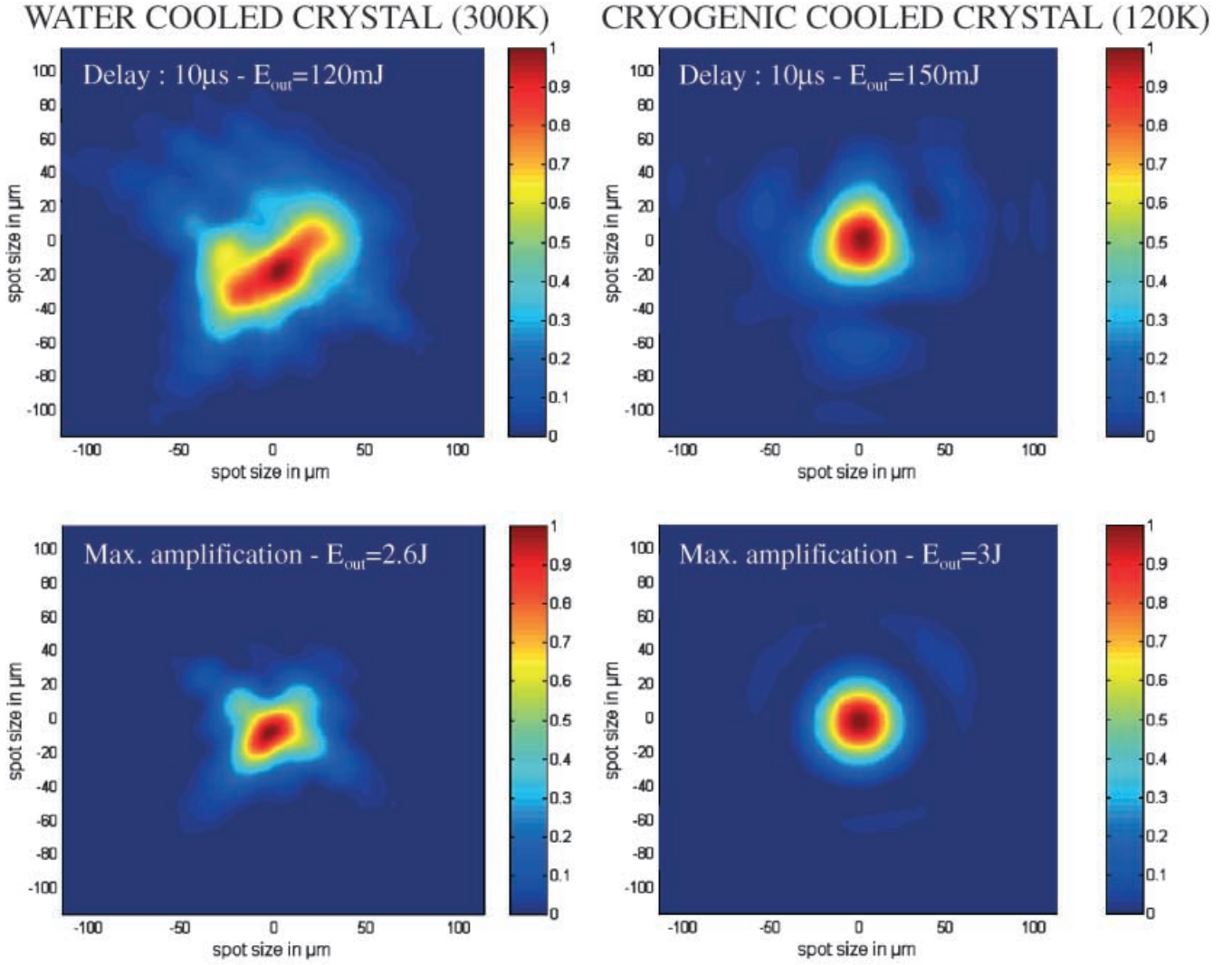


FIGURE 6 Focal spots calculated considering a 300-mm aberration-free focusing from Shack–Hartmann wavefront measurements of the amplified pulses. Measurements were made after three passes through the amplifier with an average pump power of 80 W and under two crystal cooling conditions. *Left*: water cooling (300 K), low extraction (*top*), and maximum amplification (*bottom*); *right*: cryogenic cooling (120 K), low extraction (*top*), and maximum amplification (*bottom*). These measurements evidence the strong efficiency of the cryogenic cooling by comparison with the standard water cooling in order to maintain a low thermal distortion level of the wavefront of the amplified beam

	Water cooling ($T = 300$ K)		Cryogenic cooling ($T = 120$ K)	
	IR beam delayed (10 μ s)	Maximum amplification	IR beam delayed (10 μ s)	Maximum amplification
Thermal lens effect^a				
Thermal focal length	5.6 m	7.6 m	56 m	90 m
Induced defocusing ^b		5 mm		0.37 mm
Thermal distortions				
Astigmatism	1.5λ	0.9λ	$\lambda/3$	$< \lambda/10$
Trefoil and tetrafoil ^c	$\lambda/3$	$\lambda/10$	$\lambda/3^d$	$< \lambda/16$
Strehl ratio (SR) ^e	8%	13%	52%	91%

^a Calculated for three passes through the crystal

^b Calculated for a 1000-mm focal length

^c Fifth- and seventh-order aberrations

^d No tetrafoil

^e The Strehl ratio is defined as the ratio of the peak intensity of the distorted beam over that of a beam with the same intensity profile but with a flat wavefront

TABLE 1 Thermally induced optical beam characteristics calculated from Shack–Hartmann wavefront measurements

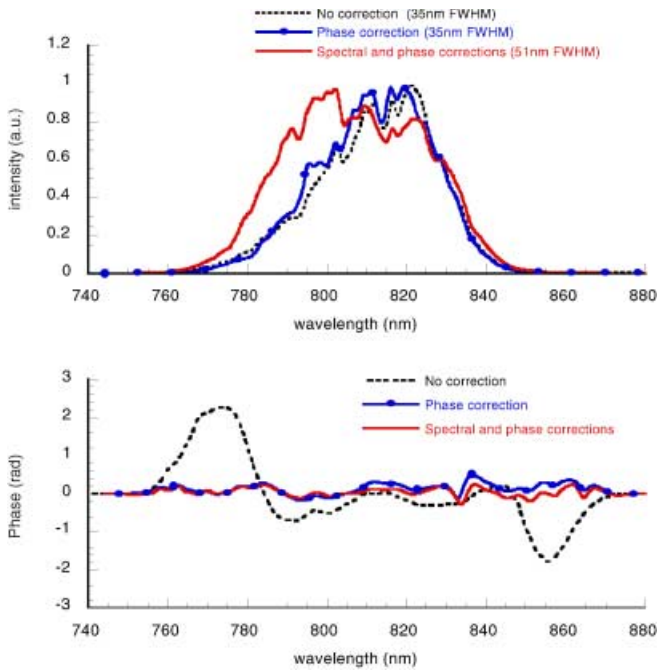


FIGURE 7 SPIDER measurements of the output amplified pulse. Each measurement was made for maximum amplification, for three different conditions: without AOPDF (---), with only phase correction (—●—), and with both amplitude and phase pre-compensation (—). *Top*: measured spectra; *bottom*: measured spectral phase

shape. This is simply obtained by digging a 50-nm large, 80% depth, Gaussian hole centered at 820 nm in the oscillator spectrum (see Fig. 3).

The spectral phase and intensity tuning was made empirically, using the real-time measurement capability of the SPIDER, in order to broaden the output spectrum while keeping a flat spectral phase. Thus, we have balanced the evolution of the spectrum through amplifiers by enhancing the blue side of the spectrum, which is less amplified than the red side because of the gain saturation, in order to obtain such a symmetric output spectral shape. This spectral broadening allowed us to further reduce the compressed pulse duration by 10%, thereby obtaining a near-Fourier-transform pulse duration of 24 fs. Moreover, as shown in the right-hand graph of Fig. 8

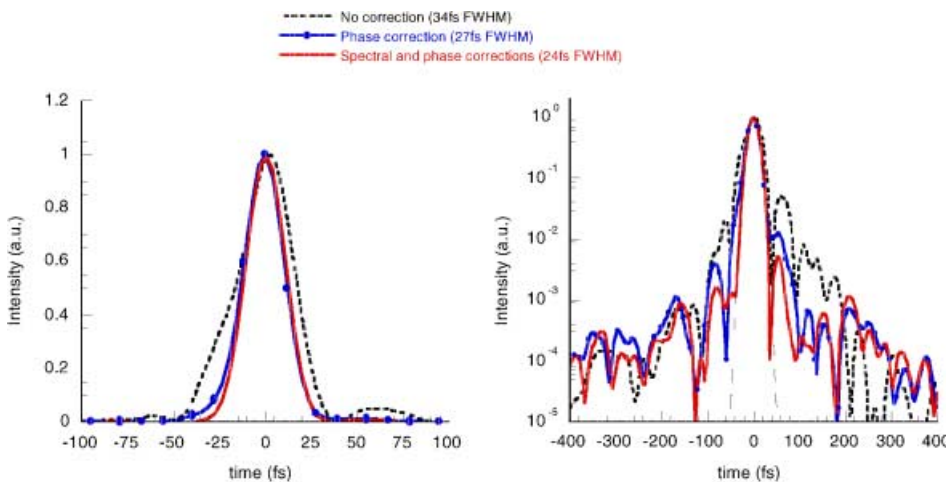


FIGURE 8 Intensity profiles calculated from SPIDER measurements of the output amplified pulses. Each measurement was made under three different conditions: without AOPDF (---), with only phase correction (—●—), and with both spectral and phase pre-compensation (—). *Left*: linear scale; *right*: logarithmic scale

on a logarithmic scale, the combination of spectral broadening and phase pre-correction increases the pulse contrast by a factor of 10 within a 200-fs window. In fact, our calculations evidence that the residual distortions in the case of the AOPDF based pre-correction are phase-independent. We believe that they are due to the existence of spectral amplitude modulations (see Fig. 7). These can be explained by the presence of a small angle between the Ti:sapphire crystals' extraordinary axis and the propagating polarization which produces dephased secondary pulses.

3.2 Spatial considerations

We measured the spatial quality of the 54-mm-diameter top-hat output beam, after compression, both with a Shack–Hartmann and with a 12-bit CCD camera. The SH gives the near-field wavefront characteristics using a $\frac{1}{12.5}$ magnification afocal system. The camera is coupled to a 20 \times objective which images the far field at the focus of a 300 mm focal length off-axis parabola to give the real intensity profile over a dynamic range of 4000 (cf. Fig. 9).

The focal spot measured with the CCD camera has a Gaussian-shape profile both in the X and Y directions with a average diameter of 5.7 μm at half-maximum, which is close to the diffraction limit. The SH measurements give a low aberration wavefront of better than 0.6λ peak-to-valley and 0.15λ rms, which lead to a PSF comparable to that measured with the CCD camera (compare up-right and down-left images in Fig. 9). Calculations give a Strehl ratio of 50%. This finally leads to intensities as high as 10^{20} W/cm² with the achieved peak-power levels of 100 TW.

4 Conclusion

We have developed and characterized a high-peak-power laser system delivering 100 TW at 10 Hz for high-field physics interactions. This system, based on the previous 30-TW Ti:sapphire CPA laser chain, is using innovative techniques for controlling temporal and spatial characteristics of the amplified beam. By implementing an acousto-optic modulator to control both spectral amplitude and phase the output-pulse duration was reduced from 34 fs down to 25 fs. We increased the output energy by increasing the pumping power of

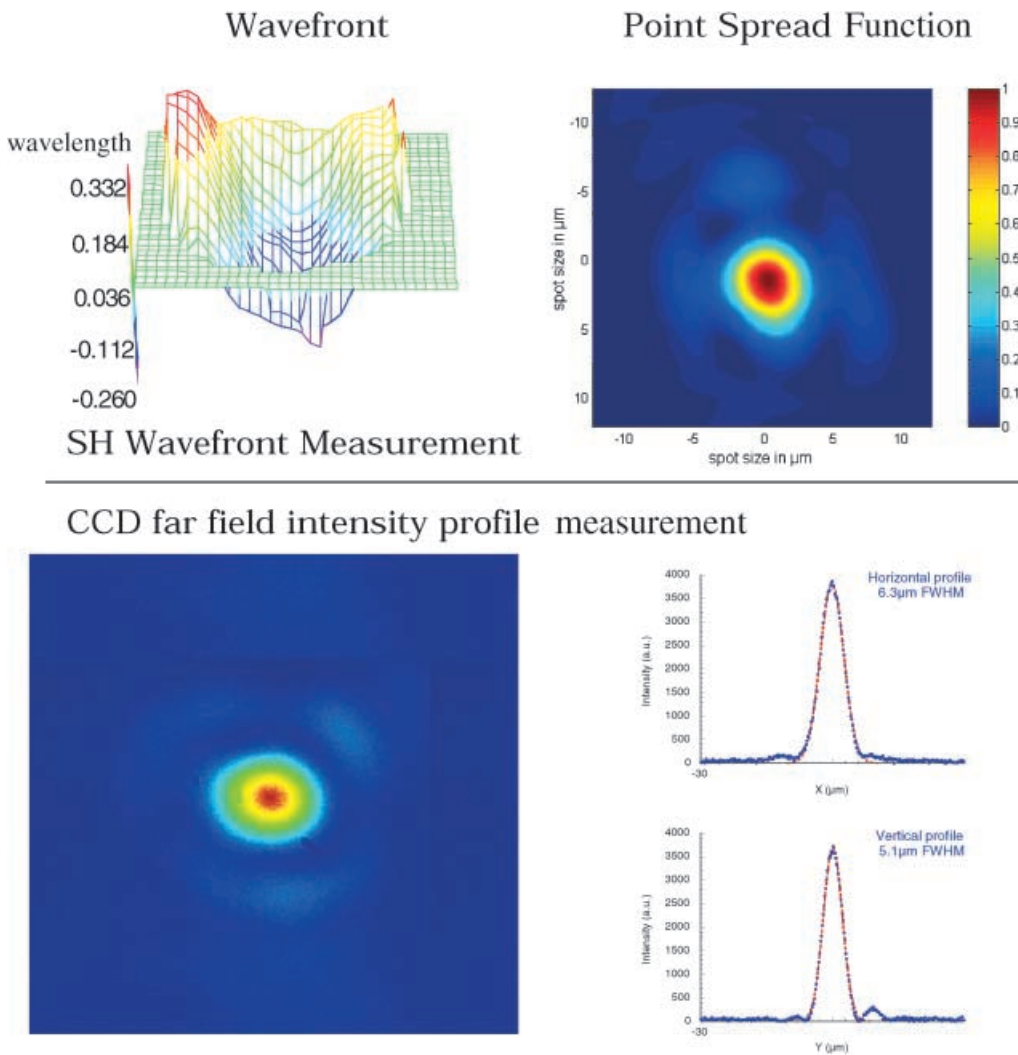


FIGURE 9 Wavefront and far field intensity profile of the compressed pulse. *Up*: Shack–Hartmann wavefront measurement (*up-left*) and corresponding calculated focal spot (*up-right*). *Down*: far field intensity profile obtained by focusing the beam with a f 300 mm/100-mm-diameter off-axis parabola and imaged with a $20\times$ objective onto a 12-bit CCD camera (*down-left*) and X , Y profiles fitted with Gaussian functions (*down-right*). The wavefront distortions are less than 0.6λ (peak-to-valley) and 0.15λ (RMS); the measured diameter is $5.7\ \mu\text{m}$ at half-maximum

the third amplifier stage from 40 W up to 100 W while reducing thermal effects by housing the Ti:Sa crystal in a cryogenic cooling chamber. The output energy of the laser is 2.5 J after compression, thus leading to the 100-TW level. With a 54-mm-diameter top-hat beam having a measured Strehl ratio of 50%, intensities as high as $10^{20}\ \text{W}/\text{cm}^2$ can be achieved by focusing with a 300-mm focal length off-axis parabola. These improvements allow us to produce pulses of extremely high temporal and spatial fidelity and thus should prove useful for investigating laser–matter interactions at high intensities.

ACKNOWLEDGEMENTS This work was supported by the European commission FIRE project, No ERBFMGECT 980095.

REFERENCES

- G.A. Mourou, C.P.J. Barty, M.D. Perry: *Phys. Today* **22** (1998)
- D. Strickland, G.A. Mourou: *Opt. Commun.* **56**, 219 (1985)
- G. Chériaux, P. Rousseau, F. Salin, J.P. Chambaret, B. Walker, L.F. DiMauro: *Opt. Lett.* **21**, 414 (1996)
- K. Yamakawa, M. Aoyama, S. Matsuoka, T. Kase, Y. Akahane, H. Takuma: *Opt. Lett.* **23**, 1468 (1998)
- B.C. Stuart, M.D. Perry, J. Miller, G. Tietbohl, S. Herman, J.A. Britten, C. Brown, D. Pennington, V. Yanovsky, K. Wharton: *Opt. Lett.* **22**, 242 (1997)
- M.D. Perry, D. Pennington, B.C. Stuart, G. Tietbohl, J.A. Britten, C. Brown, S. Herman, B. Golick, M. Kartz, J. Miller, H.T. Powell, M. Vergino, V. Yanovsky: *Opt. Lett.* **24**, 160 (1999)
- Y.H. Cha, Y.I. Kang, C.H. Nam: *J. Opt. Soc. Am. B* **16**, 1220 (1999)
- J.P. Chambaret, C. Le Blanc, G. Chériaux, P. Curley, G. Darpentigny, P. Rousseau, G. Hamoniaux, A. Antonetti, F. Salin: *Opt. Lett.* **21**, 1921 (1996)
- A. Antonetti, F. Blasco, J.P. Chambaret, G. Chériaux, G. Darpentigny, C. Le Blanc, P. Rousseau, S. Ranc, G. Rey, F. Salin: *Appl. Phys. B* **65**, 197 (1997)
- S. Ranc, G. Chériaux, S. Ferré, J.P. Rousseau, J.P. Chambaret: *Appl. Phys. B* **70** [Suppl.], S181 (2000)
- F. Verluise, V. Laude, Z. Cheng, C. Spielmann, P. Tournois: *Opt. Lett.* **25**, 575 (2000)
- F. Verluise, V. Laude, J.P. Huignard, P. Tournois, A. Migus: *J. Opt. Soc. Am. B* **17**, 138 (2000)
- P.F. Moulton: *J. Opt. Soc. Am. B* **3**, 125 (1986)
- P. Albers, E. Stark, G. Huber: *J. Opt. Soc. Am. B* **3**, 134 (1986)
- C. Dorrer, B. De Beauvoir, C. Le Blanc, S. Ranc, J.P. Rousseau, P. Rousseau, J.P. Chambaret, F. Salin: *Opt. Lett.* **24**, 1644 (1999)
- C. Dorrer, B. De Beauvoir, C. Le Blanc, J.P. Rousseau, S. Ranc, P. Rousseau, J.P. Chambaret, F. Salin: *Appl. Phys. B* **70** [Suppl.], S77 (2000)